JCI insight

High protein feeding induces *de novo* lipogenesis in healthy humans: a randomised 3-way crossover study

Evelina Charidemou, … , Elise Orford, Julian L. Griffin

JCI Insight. 2019. https://doi.org/10.1172/jci.insight.124819.

Clinical Medicine In-Press Preview **Metabolism**

BACKGROUND. Dietary changes have led to a growing prevalence of Type 2 diabetes and non-alcoholic fatty liver disease. A hallmark of both disorders is hepatic lipid accumulation, derived in part from increased de novo lipogenesis. Despite high protein diets being popular for weight loss to tackle these metabolic disorders, the effect of dietary protein on *de novo* lipogenesis is poorly studied. We aimed to characterise the effect of dietary protein on*de novo* lipid synthesis.

METHODS. Herein, we use a 3-way crossover interventional study in healthy males to determine the effect of high protein feeding on *de novo* lipogenesis as well as in vitro models to determine the effects of specific amino acids on fatty acid synthesis. The primary outcome was change in *de novo* lipogenesis-associated triglycerides in response to protein feeding.

RESULTS. We demonstrate that high protein feeding, rich in glutamate, increases*de novo* lipogenesis-associated triglycerides in plasma (2-fold compared to Control; $p < 0.0001$) and liver-derived very low-density lipoprotein particles (1.8 fold; $p < 0.0001$) in samples from human subjects ($n = 9$ per group). In hepatocytes, we show that glutamate derived carbon is incorporated into palmitate and […]

High protein feeding induces de novo lipogenesis in healthy humans: a randomised 3-way crossover study

Evelina Charidemou[1], Tom Ashmore[1], Xuefei Li[1], Ben D McNally[1], James A West[2], Sonia Liggi[1], Matthew Harvey[3], Elise Orford[3] and Julian L Griffin[1,4]

1. Department of Biochemistry and Cambridge Systems Biology Centre, University of Cambridge, 80 Tennis Court Road, Cambridge, CB2 1GA, UK
2. Division of Gastroenterology and Hepatology, Department of Medicine, Addenbrooke's Hospital, University of Cambridge, Cambridge, CB2 0QQ, UK
3. Medical Research Council Elsie Widdowson Laboratory, 120 Fulbourn Road, Cambridge, CB1 9NL, UK
4. Computational and Systems Medicine, Surgery and Cancer, Imperial College London, Exhibition Road, London, SW7 2AZ.

Corresponding Author Contact Information:
Julian L. Griffin; Department of Biochemistry, University of Cambridge, 80 Tennis Court Road, Cambridge, CB2 1GA, United Kingdom; Tel: +44 (0) 1223 764922; jlg40@ cam.ac.uk

The authors have declared that no conflict of interest exists.

Abstract

BACKGROUND. Dietary changes have led to a growing prevalence of Type 2 diabetes and non-alcoholic fatty liver disease. A hallmark of both disorders is hepatic lipid accumulation, derived in part from increased de novo lipogenesis. Despite the popularity of high protein diets for weight loss, the effect of dietary protein on de novo lipogenesis is poorly studied. We aimed to characterise the effect of dietary protein on de novo lipid synthesis.

METHODS. We use a 3-way crossover interventional study in healthy males to determine the effect of high protein feeding on de novo lipogenesis, combined with in vitro models to determine the lipogenic effects of specific amino acids. The primary outcome was a change in de novo lipogenesis-associated triglycerides in response to protein feeding.

RESULTS. We demonstrate that high protein feeding, rich in glutamate, increases de novo lipogenesis-associated triglycerides in plasma (1.5-fold compared to Control; $p < 0.0001$) and liver-derived very low-density lipoprotein particles (1.8 fold; $p < 0.0001$) in samples from human subjects ($n = 9$ per group). In hepatocytes, we show that glutamate derived carbon is incorporated into triglycerides via palmitate. In addition, supplementation with glutamate, glutamine and leucine, but not lysine, increases triglyceride synthesis and decreases glucose uptake. Glutamate, glutamine and leucine increase activation of protein kinase B, suggesting induction of de novo lipogenesis is via the insulin signalling cascade.

CONCLUSION. These findings provide mechanistic insight into how select amino acids induce de novo lipogenesis and insulin resistance, suggesting that high protein feeding to tackle diabetes and obesity requires greater consideration.

FUNDING. The research was supported by grants MR/P011705/1, MC_UP_A090_1006 and MR/P01836X/1. JLG is supported by the Imperial Biomedical Research Centre, NIHR.

Introduction

Recent rapid changes in diet have coincided with modernisation, urbanisation, economic development, and increased population wealth, and have had a profound effect on body composition and health status (1). The transition from traditional diets, high in cereal and fibre, to 'Western-style' diets high in sugars, fat, and animal-derived products are thought to be key contributors to the obesity epidemic and increased incidences of metabolic syndrome, type 2 diabetes (T2DM) and non-alcoholic fatty liver disease (NAFLD) (2).

Both NAFLD and T2DM (3) have been associated with increased hepatic lipid production via de novo lipogenesis (DNL). This pathway synthesises "new" fat, utilising acetyl-coenzyme A (CoA) as a carbon source, derived from a number of metabolic reactions including glycolysis or the deamination of amino acids. Fatty-acyl chains can then be incorporated into a variety of lipid species, including triacylglycerols (TAG) and phospholipids. The pathway commences by carboxylation of acetyl-CoA to malonyl-CoA by acetyl-CoA carboxylase (ACC). Malonyl-CoA is then transferred to a complex multifunctional enzyme, fatty acid synthase (FAS). Multiple rounds of activation of acetyl-CoA to malonyl-CoA, transferral to FAS and addition to the lengthening carbon chain generate palmitate (4).

DNL is regulated at a transcriptional level by both glucose and insulin. It has previously been established that hyperinsulinaemia and high carbohydrate diets "prime" DNL by providing a large substrate pool (5, 6). Glucose also stimulates the expression of anabolic DNL genes, including those encoding ATP-citrate lyase (ACL), ACC and FAS (*ACLY*, *ACACA* and *FASN*, respectively) by the action of the transcription factor, carbohydrate response element binding protein (ChREBP) (7). In turn, insulin activates the same genes, via protein kinase B/AKT2 (8), by the action of sterol

regulatory binding protein 1c (SREBP-1c), one of two transcripts produced from the sterol response element-binding protein gene. Once fatty acids (FAs) are synthesised, they are subsequently desaturated via the action of stearoyl-CoA desaturase 1 (SCD1), and/or elongated, by elongation of very long fatty acids protein 6 (ELOVL6). Finally, fatty acids may be incorporated into TAGs and packaged into very low density lipoproteins (VLDLs) for export.

Accumulation of a subset of shorter chain TAGs (scTAGs) and VLDL-associated scTAGs in the liver and blood, respectively, has been associated with DNL and hepatic steatosis (9). In healthy humans, the amount of de novo-produced TAG incorporated in VLDL is small (below 5%; (10)). However, in hyperinsulinaemic individuals with NALFD, de novo-produced TAG content increases to 26% (4). Furthermore, in healthy human subjects, feeding with a high carbohydrate meal is sufficient to increase DNL-derived TAG content to 23% (10). Whilst numerous studies have shown that high carbohydrate feeding increases DNL (11), studies of the effect of high protein feeding in relation to DNL in humans are limited.

The branched-chain amino acids (BCAAs), leucine, isoleucine and valine, are known to correlate with insulin resistance and T2DM in humans (12). Studies have demonstrated that deprivation of BCAAs from the diet whilst maintaining levels of other amino acids is sufficient to improve glycaemic control (13). Increased circulating BCAAs are sensed by mammalian target of rapamycin (mTOR), a protein kinase which is a critical node of the insulin signalling cascade, and subsequently promote DNL (14). Hyperactivation of the mTOR pathway by excessive amino acid concentrations leads to the phosphorylation of multiple serine residues within, and subsequent inactivation of, the insulin receptor substrate 1 (IRS-1) (15). This results in a weakened response to insulin, progressing to persistent insulin resistance. Despite this, high

protein/low carbohydrate diets are popular regimes for weight loss in humans and dietary protein has been shown to decrease hepatic lipid accumulation in rodents (16). Presently, the precise amino acid components that are responsible for these effects, and the extent to which amino acids are able to induce DNL and VLDL secretion are not known.

The primary objective of this study was to characterise the effect of dietary amino acids on DNL. We demonstrate that high protein feeding, using a soy protein intervention rich in glutamate, results in increased levels of scTAGs and VLDL-associated scTAGs, that have been associated with DNL (9), in plasma of human male subjects. Only males were recruited due to the large difference between the lipid profiles of men and pre-menopausal women arising from different sex hormones, which are important regulators of lipid metabolism (17). We also determine that glutamate induces DNL and is itself incorporated in fatty acids via the TCA cycle in hepatocytes, most likely via reductive carboxylation. In addition, supplementation with the BCAA leucine and glutamine in hepatocytes resulted in a significant increase in scTAGs as well as a decrease in glucose uptake. This may provide insight into the negative effects of BCAAs on insulin sensitivity and metabolic health, and was recapitulated in both glutamine and glutamate but not lysine supplementation.

Results

scTAGs are major discriminant variables between high protein- and *control-fed healthy male subjects*

Nine healthy male subjects completed the trial protocol (Figure 1); baseline characteristics for these volunteers are summarised in Table 1. The subjects consumed an isoenergetic (2 MJ) control meal (C), high protein meal (HP) and a high fat meal (HF), and plasma samples were collected hourly over 6 h. To assess changes in the plasma triglyceride profiles obtained by LC-MS, data were processed by constructing Principal Components Analysis (PCA) models to identify the distribution of the variables and remove any outliers detected using the Hotelling's T2 test. Subsequently, orthogonal projections to latent structures discriminant analysis (OPLS-DA) models were created to discriminate between the three groups. In the OPLS-DA models, time points T3, T4 and T5 were utilised as this provided sufficient time for ingested macronutrients to reach the extrahepatic blood (18). OPLS-DA readily separated the HP group from the C group ($R^2X = 0.84$, $Q^2 = 0.47$; Figure 2A). However, there was a less clear separation between the HP group from the HF group ($R^2X = 0.54$, $Q^2 = 0.32$; Figure 2B). Both models were validated using permutation tests, yielding R^2X and Q^2 ($R^2 = (0.0, 0.56)$, $Q^2 = (0.0, -0.63)$; $R^2 = (0.0, 0.21)$, $Q^2 = (0.0, -0.30)$ respectively) lower than the original, hence indicating stable and non-random models (Figure 2C & D). Cross validation analysis of variance (CV-ANOVA) also showed a significant *p*-value for both models ($p = 0.0063$ and $p = 0.0032$, respectively). The loadings plot of the C *versus* HP model was then used to determine the metabolite features that differ between the groups (Figure 2E). Variable importance on projection (VIP) was utilised to filter important metabolites in the model. The vectors in the projection are regularised such that, if all variables were of equal importance, their

values would be equal to 1. Therefore, any variable with a VIP value greater than 1 was considered to be a potential discriminant variable. TAGs containing shorter and more saturated fatty acids (red circles; Figure 2E) were the major VIPs increased in the HP group (Figure 2F).

The TAG profiles were further analysed by hierarchical clustering, and heatmap representations were obtained from the Spearman correlation matrix among metabolites. One of the clusters contained scTAGs with more saturated fatty acids, indicating that changes in TAG levels were consistent within members of the cluster, with these scTAGs having been previously correlated with DNL and steatosis, as well as cardiovascular disease (19) and risk of developing type 2 diabetes (20) (Supplemental Figure 1).

HP feeding in healthy male subjects increases scTAGs in both plasma and the LDL/VLDL fraction.

The total amount of triglycerides was not significantly different between the three groups (Figure 3A). However, total scTAGs were markedly elevated in HP-fed subjects 3 h post-feeding compared to the same individuals fed with the C or HF meal (Figure 3B). After an overnight fast and subsequent feeding with the HP meal, there was an increase in scTAGs up to 4 h compared with baseline (Figure 3B). There were no significant differences in scTAGs between the baseline and hourly samples in C- and HF-fed subjects (Figure 3B). To determine whether these TAGs were produced by the liver and not the intestine, we extracted LDL/VLDL, through a series of precipitation and low-speed centrifugation steps and analysed their TAG profile. In line with changes in plasma, the sum of scTAGs in the LDL/VLDL fraction was higher in HP-fed subjects than C-fed subjects after 3 h (Figure 3C). Fatty acids from the meal as well as free fatty acid (FFA) are major precursors of lipoprotein TAGs. The C and HP

meals did not have any differences in meal fatty acid compositions (Supplemental Table 1) nor in the plasma FFA content (Supplemental Figure 3), suggesting that these TAGs were synthesised de novo.

The plasma 16:0/18:2n-6 ratio was calculated as an index of DNL, since during DNL plasma TAGs are enriched with 16:0, the primary product of FAS, and depleted in 18:2n-6, an essential fatty acid (21). At 4 h, where we saw the biggest increase in scTAGs, the 16:0/18:2n-6 ratio was significantly greater after a high protein meal than after the C meal (Figure 3D).

Increases in DNL during high protein feeding may be explained by increases in insulin. However, the insulin peak at 30 min was not significantly different between C and HP (Supplemental Figure 2).

Glutamate acts as a substrate for the synthesis of triacylglycerols via the TCA cycle and DNL-derived palmitate in AML 12 hepatocytes.

Under physiological conditions carbohydrates act as the canonical source of substrate for DNL. However, the contribution of amino acids, derived from protein-rich diets, is less well understood beyond the context of oncometabolism. To determine whether amino acids act as substrates for DNL under conditions of typical carbohydrate supply (approximately 5 mmol/L), we supplemented AML 12 hepatocytes with $^{13}C_5$-labelled glutamate, the most abundant amino acid in the HP meal (Supplemental table 2), to trace its metabolic fate. The carbon backbone of glutamate may enter the TCA cycle via deamination to α-ketoglutarate. Analysis of subsequent TCA cycle intermediates using mass spectrometry showed that, compared to unlabelled samples, the levels of labelled TCA cycle intermediate citrate $[M+2]^+$ and $[M+5]^+$ (mass of the unlabelled compound plus 2 or 5 Da for the labelled carbons) were markedly increased in labelled

samples over 24 h (Figure 4). Interestingly, the $[M+4]^+$ citrate generated by the addition of unlabelled acetyl-CoA to $[M+4]^+$ oxaloacetate cannot supply $[M+2]^+$ labelled acetyl-CoA for the synthesis of fatty acids (22). Whilst citrate is chemically symmetrical, the enzymes citrate synthase (CS) and ACL are regiospecific, such that the acetyl-CoA cleaved by ACL is the same as that added by CS (23, 24). The ^{13}C label from glutamate was detected in the $[M+4]^+$ ion of palmitate, which was found to be significantly increased in labelled samples 3 h post-supplementation (Figure 5A). Once fatty acids are synthesised, they are packaged into TAGs and exported from the liver as VLDL. We further detected the label in the scTAG 48:0 both intracellularly and in the cell culture media (Figure 5B).

As such, we suggest the most likely process by which carbon from glutamate was incorporated into FAs was via reductive carboxylation in the TCA cycle. This reverse flow through the TCA cycle typically occurs during periods of decreased NAD^+ to NADH ratio, corresponding to high energy balance, which was detected in glutamate-supplemented samples compared to control (Figure 5C).

Taken together, these data suggest that not only do amino acids provide carbon for use in DNL, the levels of incorporation of amino acid-derived carbon are appreciable even in the presence of physiological glucose concentrations.

Select amino acids increase scTAGs in AML 12 hepatocytes

We next sought to determine whether amino acids increase DNL and chose representatives of glucogenic (glutamate and glutamine) and ketogenic (leucine and lysine) amino acids. We supplemented AML 12 hepatocytes with increasing concentrations of glutamate, glutamine, leucine and lysine. As expected, intracellular amino acid levels increased dose dependently in response to the corresponding amino

acid increases in media (Figure 6A). Total scTAG levels increased dose-dependently in response to glutamate, glutamine and leucine but not lysine concentrations (Figure 6B), with the greatest effect achieved by supplementation with leucine. Lysine did not increase the levels of scTAGs and in separate experiments, label from $^{13}C_6$-lysine was not detected in palmitate or palmitate-containing triglycerides (Supplemental Figure 4).

Glutamate increases the expression of DNL genes

The synthesis of VLDL particles may be separated into 3 main processes: synthesis of fatty acids, elongation and desaturation of fatty acids, and packing of fatty acids into triacylglycerols and VLDL. Synthesis of fatty acids is initiated by ATP-citrate lyase (*Acly*), responsible for lysing citrate to acetyl-CoA. Acetyl-CoA is then carboxylated to malonyl-CoA, via acetyl-CoA carboxylase (*Acaca*), which is subsequently utilised by a multifunctional enzyme, fatty acid synthase (*Fasn*), to synthesise fatty acids. Increasing levels of glutamate elevated the expression of *Acly* and *Fasn* dose-dependently, with a significant increase at 10 mmol/L glutamate after 24 h (Figure 7A). However, there were no changes in the expression of *Acaca*. Once synthesised, palmitate may be desaturated and/or elongated to palmitoleate and stearate by stearoyl-CoA desaturase 1 (*Scd1*) and elongation of very long fatty acids protein 6 (*Elovl6*), respectively. Glutamate increased the expression of *Scd1* (10 mmol/L glutamate) and *Elovl6* (4 and 10 mmol/L glutamate; Figure 7B). Fatty acids are then sequentially esterified to glycerol to form triglycerides, with the terminal step catalysed by diacylglycerol O-acyltransferase 2 (*Dgat2*). The microsomal triglyceride transfer protein (*Mttp*) is then responsible for shuttling triglycerides through membranes such that they may associate with apolipoprotein B100 and apolipoprotein C-III (*Apoc3*).

Glutamate at 10 mmol/L increased the expression of *Dgat2* and *Apoc3* but not *Mttp* (Figure 7C).

Profile of expression of DNL genes in response to amino acid supplementation

Glutamine at 2 and 4 mmol/L increased the expression of the fatty acid synthesis genes (*Acly* and *Fasn*, but not *Acaca)*, processing and packaging genes (Figure 8A). However, at 10 mmol/L glutamine, the expression of *Fasn* and *Elovl6* was no longer significantly increased. Despite leucine resulting in the greatest increase in scTAGs in hepatocytes, it decreased the expression of fatty acid synthesis (except *Acaca*) and processing genes, with significant changes at 10 mmol/L leucine. However, it increased the expression of packaging genes dose-dependently (Figure 8B). Lysine did not change the expression of any genes significantly, in agreement with the finding that lysine did not affect scTAG content in hepatocytes (Figure 8C).

Glutamate, glutamine and leucine increase phosphorylation of *AKT*

Through a partially characterised mechanism, insulin activates the transcription factor SREBP1c to induce the expression of genes required for hepatic DNL. A key node in this signalling cascade is PKB/AKT2, a protein kinase that transduces the signal to downstream effectors, such as mTOR complex 1 (mTORC1). It is known that amino acids activate mTORC1, however, it has only recently been reported that mTORC1 activation in the absence of PKB/AKT2 is not sufficient to stimulate SREBP1c and thus DNL (25). We therefore investigated whether amino acids can act upstream of mTORC1 and activate PKB/AKT2 by quantifying the levels of the active kinase, as a ratio to total PKB/AKT2, via measuring phosphorylation at Ser 473. In AML12 hepatocytes, intracellular pPKB/AKT2 levels increased dose-dependently in response

to glutamate (4 and 10 mmol/L), glutamine (10 mmol/L) and leucine (4 and 10 mmol/L) but not lysine concentrations (Figure 9).

Glutamine and leucine decrease glucose uptake in AML12 hepatocytes

As insulin resistance is thought, at least in part, to result from the hyperactivation of mTOR and the subsequent phosphorylation of IRS1 (26) , we sought to determine the acute effects of amino acid supplementation on the uptake of the glucose analogue, 2-deoxyglucose. This molecule is recognised by glucose transporters, phosphorylated within the cell by glucokinase but cannot be further metabolised and is thus sequestered within the cell. Upon addition of 2-deoxyglucose, insulin-stimulated uptake was significantly lower in both glutamine- and leucine-supplemented cells (Figure 10A and 10B, respectively), but not with lysine (Figure 10C).

Discussion

The latest nutritional transition from traditional to western-style diets (rich in sugar, fat and protein from red meat) has led to a growing prevalence of NAFLD and T2DM (3). Hepatic lipid accumulation, in part via upregulated levels of DNL, is mutual to both disorders. Whilst it is well established that high carbohydrate feeding increases DNL (11), studies of the effect of high protein feeding in relation to DNL in humans, are limited. Despite high protein/low carbohydrate diets being popular regimes for weight loss in humans to prevent obesity and diabetes, recent studies correlated elevated BCAA levels with insulin resistance and T2DM (12). The precise dietary amino acid composition that may induce DNL is, as yet, unknown.

In the present 3-way cross over study, healthy human males consumed three meals (C, HP and HF) in a randomised order. Only young healthy males were included in this study as pre-menopausal females have more variable lipid profiles due to the effects of oestrogen and as we were limited in sample size by cost and time constraints we chose to focus on males for this study. As the volunteers are healthy, the effects observed are a consequence of the parameters of the study, without the confounding factor of disease status or variability in lipid profile. In addition, the meals were designed such that all three meals were isocaloric. Consequently, and unavoidably, the carbohydrate content of the meals varied, which may be considered to confound the results. However, the caloric content was considered the more important determining factor in metabolic processes, including DNL, and therefore opted to make this parameter a constant 2 MJ.

Lipidomic changes were detected at hours 3, 4 and 5 postprandially, particularly in the TAG class of lipids. Using earlier time points, valid models were not generated, possibly due to the delay between intake of the meal and its subsequent effect on the

blood lipidome. Based on the initial multivariate analysis, we opted to focus on a more detailed analysis in the C and HP groups.

We show that dietary amino acids increase scTAGs, that have been previously associated with DNL, steatosis (9) and insulin resistance (20). However, it should be noted that these scTAGs are not a direct measure of DNL and this should be considered as a limitation of the study that DNL was not directly measured using stable isotope based approaches. However, we also show that palmitate may readily be derived from glutamate via DNL, suggesting that amino acids may provide carbon as a substrate for this process under physiological substrate concentrations. We determined differential effects of amino acids on scTAGs as well as the expression of genes required for synthesis, processing and packaging of fatty acids, likely involving the action of AKT2 in hepatocytes. We demonstrated that a HP meal, rich in glutamate, increased scTAGs in plasma as well as in the LDL/VLDL fraction in healthy human males. These effects were following a 12-hour fast, which typically supresses DNL (27), and so may underestimate the physiological consequences of a high protein meal in terms of DNL. Thus, these results may therefore have general implications for high-protein diets and T2DM. Studies have previously demonstrated that a higher protein/lower carbohydrate diet downregulates DNL (28, 29), typically in longer-term dietary interventions. However, the precise amino acid composition of the high protein diet was not determined, and as we show herein, activation of DNL is specific to certain amino acid treatments. The precise metabolic parameters and time-frame of these effects on DNL remain to be fully elucidated.

A master regulator of cell growth, mTORC1, is responsible for sensing nutrient signals, particularly amino acids (30). The mTORC1 signalling pathway integrates insulin signals, through its phosphorylation by PI3-kinase/AKT2 (31). Activation of mTORC1

leads to the nuclear localisation of liver X receptor alpha (LXRα), whereupon it heterodimerises with the retinoid X receptor (RXR) to induce the expression of lipogenic genes as well as SREBP1c (32). mTORC1 also mediates the nuclear translocation of SREBP1c, where it induces the transcription of genes required for DNL (33). However, it has recently been reported that mTORC1 activation in the absence of AKT2 is not sufficient to stimulate SREBP1c, and thus DNL (25), suggesting that amino acids regulate an upstream node in the pathway, or act in an, as yet, undetermined manner. Our data show that select amino acids, glutamate, glutamine and leucine but not lysine, activated AKT2. This may also indicate that specific amino acids may regulate mTOR complex 2 (mTORC2), responsible for the activation of AKT2 and subsequent induction in the expression of genes required for DNL, in support of a signalling pathway proposed by Tato *et al* (34). Amino acids, branched-chain in particular, have been linked with insulin resistance. The molecular basis is the activation p70 S6k by amino acids (35), a downstream kinase of mTORC1. This in turn phosphorylates the insulin receptor substrate at multiple serine/threonine residues, thereby attenuating glucose uptake. Persistent activation of p70 S6k by excessive amino acid concentrations may therefore lead to insulin resistance (26). Herein, we now demonstrate that glutamine and leucine decrease glucose uptake, whilst lysine does not.

In support of our finding that specific amino acids activate PKB/AKT2, we also demonstrate that the same amino acids increased scTAG content in hepatocytes. Leucine resulted in the greatest increase in scTAG content followed by glutamine and lastly, glutamate. Both glutamate and glutamine increased the expression of genes required for the synthesis, processing as well as packaging of fatty acids. Perhaps surprisingly, leucine and the highest concentration of glutamine decreased the

expression of genes required for synthesis and processing of fatty acids but increased the expression of genes required for packaging. This suggests a possible negative feedback mechanism, whereby accumulation of high levels of scTAGs or other intermediate species (such as fatty acyl-CoAs) in the liver inhibit the expression of these genes, but not the expression of genes required for subsequent processing and packaging. Indeed, studies demonstrate that unsaturated fatty acids lower the levels of mRNA for SREBP1c by accelerating its degradation (36), whilst longer chain polyunsaturated fatty acids are potent inhibitors of ACC (37). Our findings also suggest that fatty acid synthesis and processing genes are differentially regulated to packaging genes. SREBP1c induces the expression of genes required for the synthesis (*Acly*, *Acaca* and *Fasn*) and processing (*Scd1* and *Elovl6*) of fatty acids (38). On the other hand, packaging genes (Mttp and Apoc3) have been shown to be regulated by the Forkhead box O1 (FoxO1) transcription factor (39). FoxO1 is responsible for the expression of the gene encoding functional MTP, a protein responsible for the packaging of lipids with nascent apoB (only present in VLDL) in the endoplasmic reticulum. The action of MTP upon the growing VLDL particle is a rate limiting step in their formation and release into the blood. Elevated levels of MTP increase the secretion of VLDL by the liver and correlate with the pathophysiology of insulin resistance and T2DM (40). FoxO1 is itself negatively regulated by insulin, which causes its phosphorylation and nuclear exclusion (41, 42). In cases of impaired insulin regulation, this may result in uncontrollable levels of MTP (40) expression. The production of hepatic, but not intestinal apoCIII is also controlled by FoxO1 via the -498/-403 element in the *apoC3* promoter (41, 43). Two separate insulin signalling axes, PI3-kinase/PKB/AKT2 and MAPK(erk), may be responsible for this inhibition. While there is evidence supporting a role for both axes (44, 45), our data suggest that

PI3-kinase/PKB/AKT2 is not involved in this inhibition, as the expression of *Mttp* and *apoC3* are increased in the presence of increased PKB/AKT2. This is consistent with the work of Au *et al* that demonstrated that insulin inhibits the transcription of *Mttp* via the MAPK(erk) signalling cascade, but not that of PI-3 kinase (46). In the context of insulin resistance and the development of fatty liver via dysregulated rates of DNL, it might be considered hepato-protective to increase the rate at which liver-derived lipoproteins are exported, at least in the shorter term. However, it is unlikely that prolonged hypertriglyceridaemia, brought about by chronic insulin resistance, has equally beneficial effects on long-term metabolic health.

In summary, our data indicate that high protein feeding increases scTAG content in post-fast, healthy human male plasma, indicative of hepatic DNL, and in liver-derived lipoproteins. We also demonstrate that specific amino acids are responsible for these effects in a cell culture system. The human study utilises only 9 male subjects, this should be expanded in a larger and more diverse cohort before generalised applicability is possible. As dietary trends have shifted towards high carbohydrate/high fat consumption, and high-protein diets are popularised as healthier alternatives, the data herein suggest that this is a more complex consideration. Therefore, advocating the consumption of protein in the treatment of diabetes and obesity requires a more profound understanding of the roles of amino acids in the context of hepatic DNL in larger cohort studies.

Materials and methods

Human intervention protocol

General design

The study was divided into recruitment, pre-screening questionnaire and screening visit and three separate study days. Nine healthy, non-smoking men took part in a randomised, 3-way crossover study. Twenty-four h before each trial day, the diet and activity of each participant was monitored. On the trial day, participants attended the Medical Research Council - Elsie Widdowson Laboratory (MRC-EWL) for 7 h and received one of the three isoenergetic mixed meals in a randomized order. Nine subjects were randomised into one block. Randomisation was generated using a computerised program that generates random permutations. Volunteers were randomised in a 1:1:1 ratio, such that each volunteer consumed all three meals within a period of 6 weeks. The isoenergetic meals comprising: control (C; 15% protein, 40% Fat, 45% Carbohydrate), high protein (HP; 32% protein, 33% Fat, 35% Carbohydrate) and high fat (14% protein, 62% Fat, 24% Carbohydrate).

Screening visit

Screening measurements and a blood sample were taken during the screening visit. Participants were also requested to complete a 24-hour food diary. After an overnight 12-hour fast, anthropometric measurements were taken (weight, height and blood pressure) and a fasting blood sample was taken. The fasting blood sample was taken by venepuncture for analysis of full blood count, liver function, glucose, insulin and lipid profile, including total cholesterol, HDL, LDL and triglycerides. These measurements were used to determine whether participants met the inclusion criteria of the study (Table 2).

Study day protocol

Participants arrived in the morning after a 12-hour overnight fast. Participants were cannulated via the antecubital vein of one arm and blood samples were collected, 10 min apart. Participants then consumed, within 15 min of onset of eating, one of the isoenergetic meals. Subsequently blood samples were collected over a six-hour period. During the six-hour period, food consumption was not allowed, and only water was permitted *ad libitum* after 3 h had elapsed. Blood samples were collected at 12 time points at various intervals throughout the 6-hour period (T1 - T6) to perform mass spectrometry and determine blood lipid changes after a high protein meal.

LDL/VLDL purification

Purified LDL/VLDL fractions were obtained using a LDL/VLDL Purification kit (Ultracentrifugation free; Cell Biolabs, Inc.). To 200 µL of plasma on ice, 10 µL of dextran solution and 100 µL of precipitation solution A were added. The samples were incubated for 5 min on ice before centrifuging (6000 x g) for 10 min at 4°C. The remaining pellet (containing LDL/VLDL) was resuspended in 80 µL of bicarbonate solution and centrifuged (6000 x g) for 10 min at 4°C. The supernatant was transferred to a new tube and mixed thoroughly with 1 mL of 1X precipitation solution B and centrifuged (6000 x g) for 10 min at 4°C. The pellet was resuspended in 40 µL of 5% sodium chloride solution, mixed thoroughly with 1 mL of 1X precipitation solution C and centrifuged (6000 x g) for 10 min at 4°C. The above step was repeated, and the pellet resuspended in 100 µL of sodium chloride solution. To the mixture 16 µL was added of dextran removal solution before incubating for 1 h at 4°C and then centrifuging (6000 x g) for 10 min at 4°C. The supernatant (containing purified LDL/VLDL) was recovered and stored at -80°C. After acquiring the purified mixture of

LDL/VLDL fractions, metabolites were extracted from these fractions as described below and analysed by LC-MS of the lipid fraction.

Metabolite extractions

Metabolites were extracted from blood plasma/cells using the modified method of Folch and colleagues (47). Briefly, 15 µL of blood plasma or pelleted cells were mixed with chloroform/methanol (2:1, 750 µL); including a mixture of internal standards labelled with deuterium (TAGs 45:0-d29, 48:0-d31 and 54:0-d35; Qmx Laboratories Ltd.). Samples were sonicated for 15 min and water was added (300 µL). Samples were then centrifuged at 13,000 x *g* for 20 min. The organic (upper layer) and aqueous phases (lower layer) were separated. The organic samples, containing the lipid extracts, were dried under a stream of nitrogen gas whilst the aqueous samples were dried in a CentriVap Centrifugal Concentrator with attached cold trap (78100 series, Labconco Co.).

LC-MS of the organic fractions

The organic fraction was reconstituted in 100 µL chloroform/methanol (1:1), and 10 µL added to 90 µL IPA/acetonitrile/water (2:1:1). Analysis of the fractions was performed using a LTQ Orbitrap Elite Mass Spectrometer (Thermo Scientific). In positive mode, 5 µL of sample were injected onto a C18 CSH column, 1.7 µM pore size, 2.1 mm x 50 mm, (Cat # 186005296, Waters) which was held at 55°C in a Dionex Ultimate 3000 ultra-high performance liquid chromatography system (UHPLC; Thermo Scientific). A gradient (flow rate 0.5 mL/min) of mobile phase A (acetonitrile/water 60:40, 10 mmol/L ammonium formate) and B (LC–MS-grade acetonitrile/isopropanol 10:90, 10 mmol/L ammonium formate) was used. In negative ion mode, 10 µL of the sample were

injected and 10 mmol/L ammonium acetate was used as the additive to aid ionisation. In both positive and negative ion mode, the gradient began at 40% B, increased to 43% B at 0.8 min, 50% B at 0.9 min, 54% B at 4.8 min, 70% B at 4.9 min, 81% B at 5.8 min, spiked at 99% B at 8 min for 0.5 min, and subsequently returned to the starting conditions for another 1.5 min to re-equilibrate the column. The HPLC was coupled to an electrospray ionisation (ESI) source before entering the mass spectrometer. The data were collected in both positive and negative ion mode with a mass range of 110–2000 *m*/*z*. Default instrument-generated optimisation parameters were used. Tandem MS was performed, using normalised collision energy, to fragment intact lipids listed in Supplemental Table 3, in order to identify the fatty acyl chains contained within.

Picolinyl ester fatty acid derivatisation of organic fractions for LC-MS

Picolnyl esters of fatty acids (PEFAs) were produced using a modification to a method published previously (48) to measure total fatty acid content. To each dried organic extract 200 µL of 10 µmol/L deuterated internal standard mix (containing FAs 13:0, 15:0, 17:0 and 20:0) were added and dried under nitrogen. Each sample was fully resuspended in 200 µL of oxalyl chloride (2 mol/L in dichloromethane, Cat. # 310670, Sigma-Aldrich) and incubated at 65 °C in a heating block for 10 min; achieving cleavage of fatty acids from complex lipids and activating the carboxylic group. Samples were then dried under nitrogen, resuspended in 200 µL dichloromethane (Cat. # 270997, Sigma-Aldrich), and dried again. Each dried residue was then resuspended in 150 µL of 1% 3-hydroxymethylpyridine (Cat. # P66807, Sigma-Aldrich) in acetonitrile and incubated at room temperature for 5 min to produce derivatised fatty acids. The dichloromethane resuspension was repeated to ensure unreacted 3-

hydroxymethylpyridine had evaporated, dried under nitrogen and stored at -80 °C until analysis.

Analysis of total fatty acids by triple quadrupole-mass spectrometry

PEFAs were reconstituted in 100 µL 2:1 methanol:water and sonicated for 15 min. Samples were then centrifuged for 15 min at 13,000 x *g* to pellet any remaining debris. A 2 µL injection volume of the resulting solution was analysed on a TSQ Quantiva™ Triple Quadrupole mass spectrometer attached to a Vanquish ultra-high performance liquid chromatography system (UHPLC; Thermo Scientific). Chromatographic separation was achieved on an Acquity UPLC BEH C18 1.7 µm x 2.1 mm x 50 mm column (Cat # 186002350, Waters). Mobile phase A was 100% water with 0.1% formic acid and mobile phase B was 50:50 acetonitrile:isopropanol (IPA) with 0.1% formic acid. The chromatography gradient started at 30% B for 2.33 min, increased to 100% B over 1.34 min and decreased to 30% B for 1.23 min (to re-equilibrate the column) at a flow rate of 0.735 mL/min. Default instrument-generated optimisation parameters were used. Xcalibur Software (Thermo Scientific) was used to identify peaks, process mass spectra and normalise data to the closest-eluting internal standard.

Data processing for open-profiling lipidomics

Samples obtained from human subjects were acquired in two analytical batches with the analytical method described above, along with a set of quality controls (QCs, obtained by pooling 15 µL of all samples). The resulting raw data files were converted into mzML format using the tool MSconvert of the Proteowizard software (49, 50), and further processed within the R environment (51) with the libraries IPO, XCMS and CAMERA (52–54) to perform parameter optimisation based on the QC samples, peak

extraction, grouping, retention time correction, and annotation of adducts and isotopes. The output from these pre-processing steps was exported as csv file and imported into an adapted implementation of the KniMet (55) pipeline for post-processing. The LOESS batch correction utility was used to normalise for differences among the two analytical batches (based on QCs for intra-batch correction, and on all samples for inter-batch). Features were filtered firstly based on their presence in the QC samples on the two separate batches with the QC-based feature filtering functionality (thresholds for missing values and relative standard deviation (RSD)/ coefficient of variation (CV) = 50% and 20%, respectively), while median peak area comparison, as previously described by Dunn and co-workers (56), was used on the merged dataset. A summary of the CVs for key lipids are presented in supplementary table 3. Metabolites were annotated based on accurate mass using a library built from the LIPID MAPS mass spectrometry combinatorial expansion package (57). Finally, the data matrix to be utilised for multivariate statistical analysis was subjected to missing values imputation with the KniMet MVI-KNN tool.

Growth of AML 12 hepatocytes

Alpha mouse liver 12 (AML 12) cells were purchased from American Type Culture Collection (ATCC) and cultured in 1:1 Dulbecco's modified Eagle's medium and Ham's F12 medium (Thermo), supplemented with 10% fetal bovine serum (FBS), 1% penicillin/streptomycin (100 units/mL and 100 µg/mL, respectively), 1% Insulin-Transferrin-Selenium (ITS; 10 mg/L, 5.5 mg/L and 6.7 µg/L respectively) and dexamethasone (100 µmol/L) at 37°C in 5% CO_2. Cells were removed from liquid nitrogen, thawed rapidly and initially cultured in a T25 flask (Cat. # 690175, Greiner). Medium was changed every two days, and upon reaching confluence, cells were sub-

cultured in T75 flasks (Cat. # 7340290, VWR) at a ratio of 1:3. Cells were plated at a density of 50,000 cells/well in collagen 1-coated 12-well plates (Cat. # 7340295, VWR) and grown to confluence in maintenance medium. Cells were then supplemented with low glucose (7.60 mmol/L) with unlabelled L-glutamate (4 mmol/L) and dialysed FBS (Thermo) for 2 days. After switching medium, cells were serum-starved for 20 h in low glucose medium supplemented with unlabelled L-glutamate (4 mmol/L).

AML 12 cell $^{13}C_5$-^{15}N-L-glutamate labelling procedure

Cells were supplemented with glucose (7.60 mmol/L, *n*=3) with unlabelled-L-glutamate (4 mmol/L) or glucose (7.60 mmol/L, *n*=3) with $^{13}C_5{}^{15}N$-L-glutamate (4 mmol/L, *n*=3). Based on previous experiments, the cells were allowed 3 h such that the $^{13}C_5$-^{15}N-L-glutamate could reach an isotopic steady state in the TCA cycle. Cells and media were harvested at 0, 3 and 24 h.

Dose response of glutamate, glutamine, leucine and lysine in AML 12 hepatocytes

Cells were supplemented with low glucose (7.60 mmol/L, *n*=3) without the specific amino acid (0 mmol/L) or with increasing levels of amino acid (2, 4, 10 mmol/L, *n*=3/amino acid). Cells and media were harvested after 24 h.

Harvesting of AML12 cells for metabolomics

For cells and media undergoing metabolomic analyses, 900 µL of medium was taken from each well and frozen at -80°C. Each well was then washed with 1 mL of 0.9% saline and cells were lifted from the plates by adding 0.5 mL trypsin (10X trypsin-EDTA, Cat. # 25300045, Invitrogen). Each well was re-washed with 0.5 mL of 0.9% sterile-filtered saline and the resulting solution was transferred into a 2 mL

microcentrifuge tube and centrifuged at 13,000 x g for 10 min to pellet the cells. The supernatant was removed and the pellet was resuspended in 750 µL of a 2:1 chloroform:methanol solution to prevent enzymatic degradation of metabolites, and frozen at -80°C.

Analysis of aqueous metabolites by triple quadrupolar-mass spectrometry

Metabolites were extracted as described above and aqueous extracts were reconstituted in 50 µL of 10 mmol/L ammonium acetate in water before TCA cycle intermediates were separated using reversed phase liquid chromatography using a Vanquish UHPLC attached to a TSQ Quantiva triple quadrupole mass spectrometer (Thermo Scientific). Multiple reaction monitoring was used in conjunction with positive/negative ion mode switching utilising the optimised mass transitions. A C18-PFP column (150 mm x 2.1 mm, 2.0 µm (ACE)) was utilised at a flow rate of 0.5 mL/min, with a 3.5 µL injection volume. For chromatography on the UHPLC system, mobile phase A was 0.1% formic acid in water and mobile phase B was 0.1% formic acid in acetonitrile. The gradient started at 30% B, increased to 90% B at 4.5 min for 0.5 min and returned to the starting conditions for a further 1.5 min to re-equilibrate the column. Mass transitions of each species were as follows (precursor > product): D_5-L-proline 121.2 > 74.2; D_8-L-valine 126.1 > 80.2; D_{10}-L-leucine 142.0 > 96.2; L-glutamate [M] 148.0 > 84.2; L-glutamate [M+1] 149.0 > 85.2; L-glutamate [M+6] 154.1 > 89.1; Citrate 191.0 > 111.0; Citrate [M+1] 192.0 > 112.0; Citrate [M+2] 193.0 > 113.0; Citrate [M+3] 194.0 > 114.0; Citrate [M+4] 195.0 > 114.0; Citrate [M+5] 196.0 > 115.0; Citrate [M+6] 197.0 > 116.0. Collision energies and RF lens voltages were generated for each species using the TSQ Quantiva optimisation function. Xcalibur Software

(Thermo Scientific) was used to identify peaks, process mass spectra and normalise data to the closest-eluting internal standard.

NAD^+/NADH assay

Briefly, cells were lysed using NAD^+/NADH extraction buffer and enzymes that consumed NADH were removed by filtration through a 10 kDa spin column (Abcam, ab93349). NAD^+/NADH was measured according to the manufacturer's protocol (Abcam, ab65348).

RNA extraction and purification from AML12 hepatocytes

Total RNA was extracted and purified from hepatocytes using an RNeasy Mini Kit (QIAgen) according to the manufacturer's specifications. Purified RNA concentration was quantified at 260 nm using a NanoDrop 100 (Thermo Fisher Scientific).

cDNA production by reverse transcription

Each purified RNA sample was diluted with RNase-free water to a final concentration of 100 ng/µL. Complimentary DNA (cDNA) synthesis and genomic DNA elimination in RNA samples was performed using an RT^2 First Strand Synthesis kit (QIAgen) according to the manufacturer's specifications. The reactions were stored at -20°C prior to real time PCR analysis.

Quantitative-PCR (qPCR)

The relative abundance of transcripts of interest was measured by qPCR in RT^2 SYBR Green Mastermix (QIAgen) with a StepOnePlus detection system (Applied

Biosystems). The SYBR Green qPCR Mastermix contained HotStart DNA Taq Polymerase, PCR Buffer, dNTP mix (dATP, dCTP, dGTP, dTTP) and SYBR Green dye. Before adding cDNA to each well of the 96-well plate, cDNA was diluted in RNase-free water to final concentration 8 ng/µL. PCR component mix was prepared by mixing 10 µL SYBR Green qPCR Mastermix with 0.6 µL of 10 µmol/L target primers (forward and reverse; 6 pmoles/reaction) and 4.4 µL RNase-free water. To each well of a 96-well plate, 5 µL cDNA (total amount 40 ng) and 15 µL PCR components mix were added. The plate was centrifuged at 1000 x *g* for 30 s to ensure that the contents were mixed and to remove any bubbles present in the wells. The plate was placed in the real-time cycler with the following cycling conditions: 10 min at 95°C for 1 cycle to activate HotStart DNA Taq Polymerase; 15 s at 95°C and 1 min at 60°C to perform elongation and cooling for 40 cycles. RT^2 qPCR Primer Assays for mouse *Rn18s*, *Fasn*, *Acaca*, *Acly*, *Elvol6*, *Scd1, Dgat2, Mttp and Apoc3* were purchased from QIAgen. Expression levels were normalised to the endogenous control, *Rn18s*, using the $\Delta\Delta C_t$ method and fold changes reported were relative to the control group in the dose response (0 mmol/L 'amino acid').

Preparation of cell lysates

Cell pellets were lysed in 100 µL Cell Extraction Buffer (10 mmol/L Tris, 100 mmol/L NaCl, 1 mmol/L EDTA, 1 mmol/L EGTA, 10 mmol/L NaF, 20 mmol/L $Na_4P_2O_7$, 20 mmol/L Na_3VO_4, 1% Triton X-100, 10% glycerol, 0.1% sodium dodecyl sulfate, 0.5% deoxycholate, 1 mmol/L phenylmethylsulfonyl fluoride, complete protease inhibitor tablet and 1% of each phosphatase cocktail inhibitor 2 and 3) for 30 min, vortexing at 10-min intervals. The lysate was centrifuged at 13,000 x *g* for 10 min at 4°C and the supernatant was collected and stored at -80°C.

Cell AKT^{pS473} and AKT [total] quantification by enzyme-linked immunosorbent assay

PKB/AKT concentrations were measured using commercial assay kits (Invitrogen). The protocol was followed according to the manufacturer's specifications. The background absorbance was subtracted from all data points, including standards, and a standard curve was generated. The unknown concentrations were read from the standard curve and the concentrations were multiplied by the appropriate dilution factor. Values were normalised to protein concentration using a reducing-agent compatible bicinchoninic acid protein assay and values of AKT [pS473] were normalised to AKT [Total].

2-Deoxyglucose uptake assay

2-Deoxyglucose uptake was measured using a commercial assay kit (Abcam, ab136955). The protocol was followed according to the manufacturer's instructions.

Statistics

To calculate the sample size of the study, a paired t-test between any two comparisons with adjusted multiple comparisons was used. Based on 80% study power, and an adjusted α value 0.017, 9 subjects were needed for this study.

The distribution of the lipid species did not deviate significantly from a normal distribution (D'Agostino-Pearson omnibus normality test). Multivariate statistical analyses were performed in SIMCA-P software, Version 13.0 (Umetrics, Sweden). All variables were UV scaled and subjected to Principal Component Analysis (PCA) coupled with Hotelling's T2 test to evaluate the distribution of the observations and identify any possible outliers. Subsequently, samples were classified based on the diet

and a supervised OPLS-DA model was developed to maximise separation between the different classes. The models were validated by a permutation test (n=100) and their significance ($p \leq 0.05$) was assessed by submitting the scores of the models to a CV-ANOVA test. Loadings plots and the Variable Importance in Projection (VIP) were acquired for each model to determine which variables drive the separation between classes (threshold limit > 1.0). Once metabolites were annotated in KniMet, and analysed in SIMCA, the most discriminant variables were TAGs. Fragmentation (as described above) was performed to a group of TAGs to confirm their identity (Supplemental Spreadsheet).

These TAGs were subsequently visualised using univariate statistics. The extent to which the model fits and predicts the data is supplied by R^2X and Q^2X, respectively. For univariate statistical analyses, data were visualised using GraphPad (GraphPad Prism 5.2; GraphPad Software, San Diego, CA, USA). All data are expressed as means with the standard error of the mean (SEM). In GraphPad, 1- or 2-way analysis of variance (ANOVA) was performed where appropriate to determine significant differences between experimental groups. For 1-way ANOVA, Dunnett's post-hoc multiple comparison test was performed, whilst for 2-way ANOVA, Sidak's post hoc multiple comparison test was used. Differences between experimental groups were considered to be statistically significant when $p \leq 0.05$.

Spearman correlation among the metabolic features annotated as TAGs deriving from open-profiling lipidomics was calculated and visualised within R (51) using the cor function of the stat package and the heatmap.2 function of the gplots library (58), respectively.

Study Approval

The protocol of the present human study was approved by both the internal research review board, MRC-Elsie Widdowson Laboratory and the Cambridge South Local Research Ethics Committee, UK. Written informed consent was received from the participants prior to their inclusion in the study.

Author Contributions

EC and XL conducted the human study. EC, XL, MH and EO collected human samples. EC and SL performed data processing and analysis. EC and TA devised and conducted cell culture experiments. EC, TA, BDM and JAW performed LC-MS. XL and JLG designed the human study. EC, TA and JLG interpreted the data and wrote the manuscript.

Acknowledgements

We thank Sara Wassell for her assistance during study days, Michelle Venables and Les Bluck for study design as well as Sumantra Ray for expert technical support in the human study.

References

1. Misra A, Khurana L. Obesity and the Metabolic Syndrome in Developing Countries. *J Clin Endocrinol Metab* 2008;93:9–30.

2. Popkin BM. Global nutrition dynamics: the world is shifting rapidly toward a diet linked with noncommunicable diseases. *Am J Clin Nutr* 2006;84:289–98.

3. Bhat G, Baba CS, Pandey A, Kumari N, Choudhuri G. Life style modification improves insulin resistance and liver histology in patients with non-alcoholic fatty liver disease. *World J. Hepatol.* 2012;4(7):209–217.

4. Donnelly KL et al. Sources of fatty acids stored in liver and secreted via lipoproteins in patients with nonalcoholic fatty liver disease. *J Clin Invest* 2005;115(5):1343–1351.

5. Schwarz J, Linfoot P, Dare D, Aghajanian K. Hepatic de novo lipogenesis in normoinsulinemic and hyperinsulinemic subjects consuming high-fat, low-carbohydrate and low-fat, high-carbohydrate isoenergetic diets. *Am J Clin Nutr* 2003;77:43–50.

6. Marques-lopes I, Ansorena D, Astiasaran I, Forga L, Martínez JA. Postprandial de novo lipogenesis and metabolic changes induced by a high-carbohydrate, low-fat meal in lean and overweight men. *Am J Clin Nutr* 2001;73:253–61.

7. Kim M et al. ChREBP regulates fructose-induced glucose production independently of insulin signaling. *J Clin Invest.* 2016;126(11):4372–4386.

8. Titchenell PM et al. Direct Hepatocyte Insulin Signaling Is Required for Lipogenesis but Is Dispensable for the Suppression of Glucose Production. *Cell Metab.* 2016;23(6):1154–1166.

9. Sanders FWB et al. Hepatic steatosis risk is partly driven by increased de novo lipogenesis following carbohydrate consumption. *Genome Biol.* 2018;19:79.

10. Timlin MT, Parks EJ. Temporal pattern of de novo lipogenesis in the postprandial state in healthy men. *Am. J. Clin. Nutr.* 2005;81:35–42.

11. Hudgins LC et al. Human Fatty Acid Synthesis Is Stimulated by a Eucaloric Low Fat , High Carbohydrate Diet. *J. Clin. Invest.* 1996;97:2081–2091.

12. Würtz P et al. Metabolic Signatures of Insulin Resistance in 7,098 Young Adults. *Diabetes* 2012;61(6):1371–1380.

13. Xiao F et al. Effects of individual branched-chain amino acids deprivation on insulin sensitivity and glucose metabolism in mice. *Metabolism* 2014;63(6):841–850.

14. Crown SB, Marze N, Antoniewicz MR. Catabolism of branched chain amino acids contributes significantly to synthesis of odd-chain and even-chain fatty acids in 3T3-L1 adipocytes. *PLoS One* 2015;10(12):e0145850.

15. Tremblay F et al. Identification of IRS-1 Ser-1101 as a target of S6K1 in nutrient- and obesity-induced insulin resistance. *PNAS* 2007;104:14056–14061.

16. Schwarz J, Tomé D, Baars A, Hooiveld GJ, Müller M. Dietary Protein Affects Gene Expression and Prevents Lipid Accumulation in the Liver in Mice. *PLoS One* 2012;7(10):e47303.

17. Varlamov O, Bethea CL, Roberts CT. Sex-specific differences in lipid and glucose metabolism. *Front. Endocrinol. (Lausanne).* 2015;5:241.

18. Samson CE, Galia ALB, Llave KIC, Zacarias MB, Mercado-Asis LB. Postprandial Peaking and Plateauing of Triglycerides and VLDL in Patients with Underlying Cardiovascular Diseases Despite Treatment. *Int J Endocrinol Metab* 2012;10(4):587–593.

19. Stegemann C et al. Lipidomics profiling and risk of cardiovascular disease in the prospective population-based bruneck study. *Circulation* 2014;129(18):1821–1831.

20. Rhee EP et al. Lipid profiling identifies a triacylglycerol signature of insulin

resistance and improves diabetes prediction in humans. *J. Clin. Invest.* 2011;121(4):1402–1411.

21. Chong MF et al. Parallel activation of de novo lipogenesis and stearoyl-CoA desaturase activity after 3 d of high-carbohydrate feeding. *Am. J. Clin. Nutr.* 2008;87(4):817–823.

22. Marietta MA, Srere PA, Walsh C. Stereochemical Outcome of Processing of Fluorinated Substrates by ATP Citrate Lyase and Malate Synthase. *Biochemistry* 1981;20:3719–3723.

23. Gottschalk G. The Stereospecificity of the Citrate Synthase in Sulfate-Reducing and Photosynthetic Bacteria. *Eur. J. Biochem.* 1968;5:346–351.

24. Berwick DC, Hers I, Heesom KJ, Moule SK, Tavare JM. The Identification of ATP-citrate Lyase as a Protein Kinase B (Akt) Substrate in Primary Adipocytes. *J. Biol. Chem.* 2002;277(37):33895–33900.

25. Yecies JL et al. Akt stimulates hepatic SREBP1c and lipogenesis through parallel mTORC1-dependent and independent pathways. *Cell Metab.* 2011;14(1):21–32.

26. Tremblay F, Marette A. Amino acids and insulin signaling via the mTOR/p70 S6 kinase pathway: a negative feedback mechanism leading to insulin resistance in skeletal muscle cells. *J. Biol. Chem.* 2001;276(41):38052–38060.

27. Nieminen P et al. De novo lipogenesis is suppressed during fasting but upregulated at population decline in cyclic voles. *Exp. Biol. Med.* 2016;241:882–887.

28. Garcia-Caraballo SC et al. Prevention and reversal of hepatic steatosis with a high-protein diet in mice. *Biochim. Biophys. Acta* 2013;1832:685–695.

29. Margolis LM et al. Calorie Restricted High Protein Diets Downregulate Lipogenesis and Lower Intrahepatic Triglyceride Concentrations in Male Rats. *Nutrients* 2016;8:571.

30. Yoon MS, Choi CS. The role of amino acid-induced mammalian target of rapamycin complex 1 (mTORC1) signaling in insulin resistance. *Exp. Mol. Med.* 2016;48(1):e201-6.

31. Vinod PKU, Venkatesh KV. Quantification of the effect of amino acids on an integrated mTOR and insulin signaling pathway. *Mol. BioSyst.* 2009;5(10):1163–1173.

32. Hwahng SH, Ki SH, Bae EJ, Kim HE, Kim SG. Role of adenosine monophosphate-activated protein kinase-p70 ribosomal S6 kinase-1 pathway in repression of liver X receptor-alpha-dependent lipogenic gene induction and hepatic steatosis by a novel class of dithiolethiones. *Hepatology* 2009;49(6):1913–1925.

33. Peterson TR et al. mTOR Complex 1 Regulates Lipin 1 Localization to Control the SREBP Pathway. *Cell* 2011;146(3):408–420.

34. Tato I, Bartrons R, Ventura F, Rosa JL. Amino Acids Activate Mammalian Target of Rapamycin Complex 2 (mTORC2) via PI3K/Akt Signaling. *J. Biol. Chem.* 2011;286(8):6128–6142.

35. Iiboshi Y et al. Amino Acid-dependent Control of p70 s6k. *J. Biol. Chem.* 1999;274(2):1092–1099.

36. Ou J et al. Unsaturated fatty acids inhibit transcription of the sterol regulatory element-binding protein-1c (SREBP-1c) gene by antagonizing ligand- dependent activation of the LXR. *PNAS* 2001;98(11):6027–6032.

37. Brim T, Assimacopoulos-jeannet F, Corkey BE, Prentki M. Long-Chain Fatty Acids Inhibit Acetyl-CoA Carboxylase Gene Expression in the Pancreatic β-Cell Line INS-1. *Diabetes* 1997;46(25):393–400.

38. Ducheix S et al. Dietary oleic acid regulates hepatic lipogenesis through a liver X receptor- dependent signaling. *PLoS One* 2017;12(7):e0181393.

39. Sparks JD, Dongb HH. FoxO1 and hepatic lipid metabolism. *Curr Opin Lipidol* 2009;20(3):217–226.

40. Higuchi N et al. Effects of insulin resistance and hepatic lipid accumulation on hepatic mRNA expression levels of apoB, MTP and L-FABP in non-alcoholic fatty liver disease. *Exp. Ther. Med.* 2011;2(6):1077–1081

41. Kamagate A et al. FoxO1 mediates insulin-dependent regulation of hepatic VLDL production in mice. *J Clin Invest* 2008;118(6):2347–2364.

42. Altomonte J et al. Foxo1 mediates insulin action on apoC-III and triglyceride metabolism. *J Clin Invest* 2004;114(10):1493–1503.

43. West G et al. Key differences between apoC-III regulation and expression in intestine and liver. *Biochem. Biophys. Res. Commun.* 2017;491(3):747–753.

44. Liang R, Rimmelé P, Bigarella CL, Yalcin S, Ghaffari S. Evidence for AKT-independent regulation of FOXO1 and FOXO3 in haematopoietic stem and progenitor cells. *Cell Cycle* 2016;15(6):861–867.

45. Brunet A et al. Akt Promotes Cell Survival by Phosphorylating and Inhibiting a Forkhead Transcription Factor. *Cell* 1999;96:857–868.

46. Au W, Kung H, Lin MC. Regulation of Microsomal Triglyceride Transfer Protein Gene by Insulin in HepG2 Cells. *Diabetes* 2003;52:1073–1080.

47. Folch. A simple method for the isolation and purification of total lipides from animal tissue. *J. Biol. Chem.* 1957;226:497–509.

48. Li X, Franke AA. Improved LC–MS Method for the Determination of Fatty Acids in Red Blood Cells by LC–Orbitrap MS. *Anal Chem* 2011;83(8):3192–3198.

49. Holman JD, Tabb DL, Mallick P. Employing ProteoWizard to convert raw mass spectrometry data. *Curr. Protoc. Bioinforma.* 2014;17(46):1–9.

50. Kessner D, Chambers M, Burke R, Agus D, Mallick P. ProteoWizard: Open

source software for rapid proteomics tools development. *Bioinformatics* 2008;24(21):2534–2536.

51. R Core Team. R: A language and environment for statistical computing. R Foundation for Statistical Computing. 2017.

52. Libiseller G et al. IPO: A tool for automated optimization of XCMS parameters. *BMC Bioinformatics* 2015;16(118).

53. Smith CA, Want EJ, O'Maille G, Abagyan R, Siuzdak G. XCMS: Processing mass spectrometry data for metabolite profiling using nonlinear peak alignment, matching, and identification. *Anal. Chem.* 2006;78(3):779–787.

54. Kuhl C, Tautenhahn R, Böttcher C, Larson TR, Neumann S. CAMERA: An integrated strategy for compound spectra extraction and annotation of liquid chromatography/mass spectrometry data sets. *Anal. Chem.* 2012;84:283–289.

55. Liggi S et al. KniMet : a pipeline for the processing of chromatography – mass spectrometry metabolomics data. *Metabolomics* 2018;14(4):52.

56. Dunn WB et al. Procedures for large-scale metabolic profiling of serum and plasma using gas chromatography and liquid chromatography coupled to mass spectrometry. *Nat. Protoc.* 2011;6(7):1060–1083.

57. Sud M, Fahy E, Subramaniam S. Template-based combinatorial enumeration of virtual compound libraries for lipids. *J. Cheminform.* 2012;25(1):23.

58. Warnes GR et al. Package "gplots": Various R programming tools for plotting data. Version 3.0.1. R package. 2016.

59. Foodworks. High Gate Hill, Qld: Xyris Software. Version 08. 2015.

Figure legend

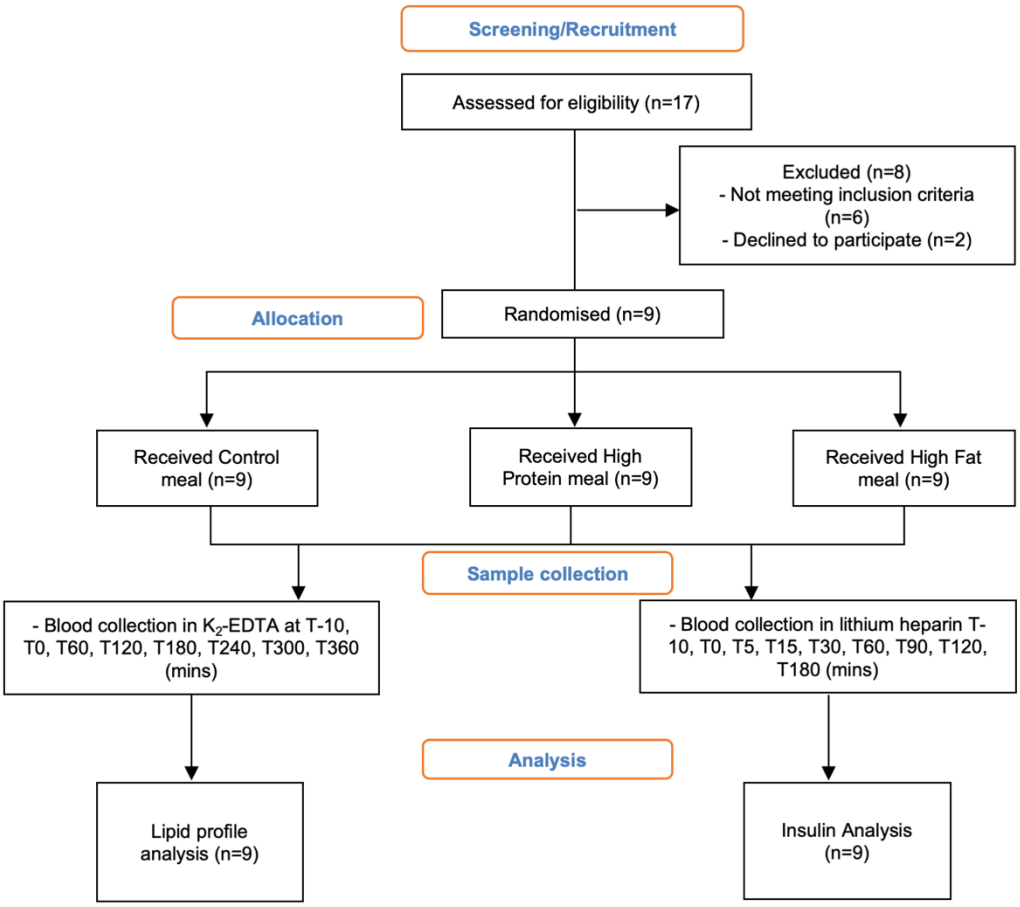

Figure 1. Study design flowchart. Seventeen males were screened to examine whether they meet the inclusion criteria of the study. Six of them did not meet the criteria and another two declined to participate. Nine volunteers participated in a randomised 3-way-cross over study. The same nine volunteers attended the Medical Research Council – Elsie Widdowson Laboratory at three different occasions and received one of the three isoenergetic meals (Control, High Protein and High Fat) in a randomised order each time. Blood samples were collected at different time points for lipid profile and hormonal analysis. The study was ended once all participants consumed the three meals.

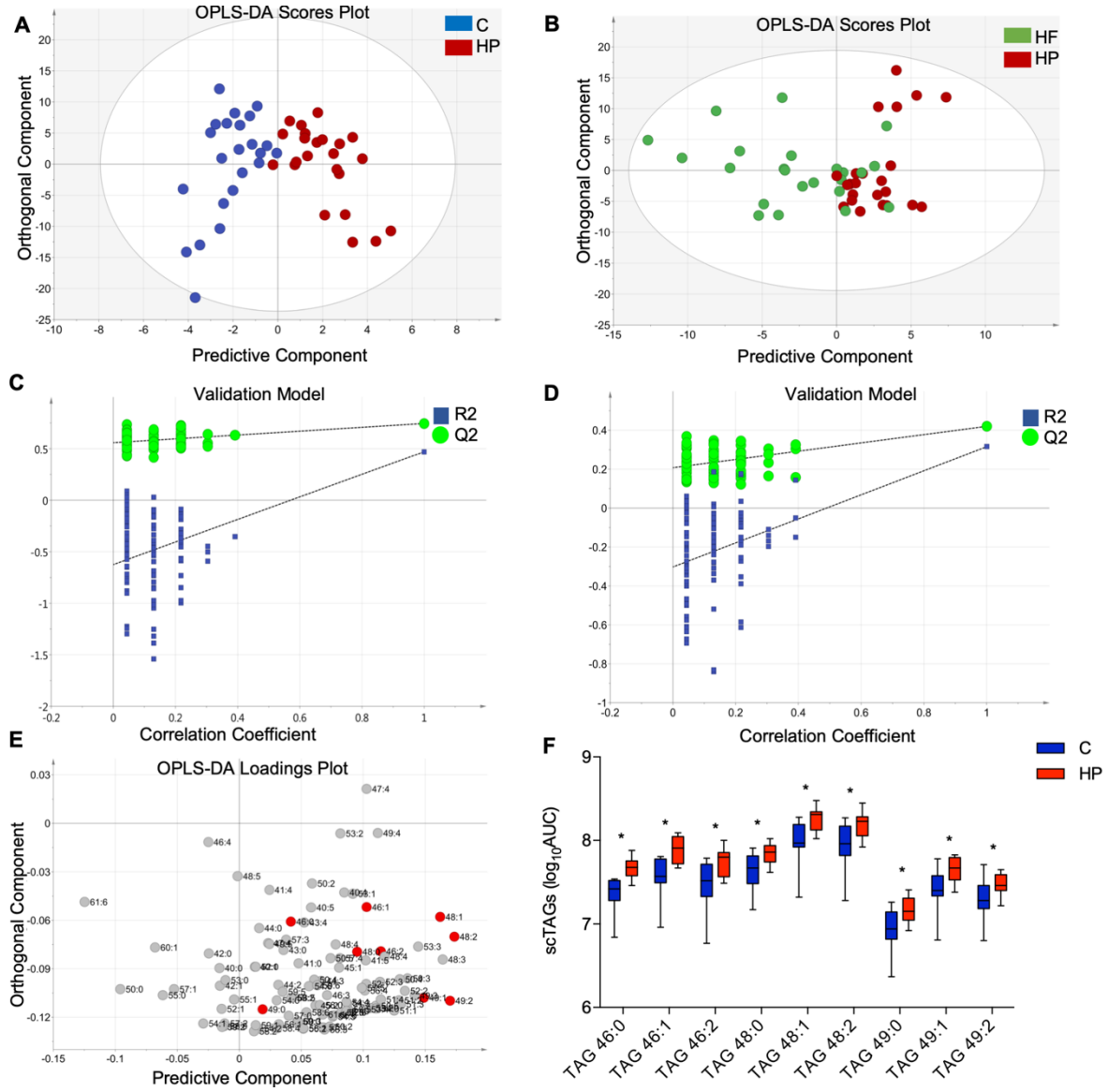

Figure 2. Multivariate data analysis of C-, HP- and HF- fed healthy human subjects. **(A)** OPLS-DA scores plot discriminating TAG profiles in plasma of C- and HP-fed individuals after 3, 4 and 5 h. Each blue circle represents a single C-fed individual, whilst red represents HP-fed individuals ($R^2X = 0.84$, $Q^2 = 0.47$). **(B)** OPLS-DA scores plot discriminating TAG profiles in plasma of HF-fed and HP-individuals after 3, 4 and 5 h. Each green circle represents a single HF-fed individual, whilst red represents HP-fed individuals ($R^2X = 0.54$, $Q^2 = 0.32$). **(C)** Cross validation of the model in **(A)** acquired through 100 permutation tests; y-axis intercepts: $R^2 = (0.0, 0.56)$, $Q^2 = (0.0, -0.63)$. *n* = 9/group. **(D)** Cross validation of model **(B)** acquired through 100 permutation tests; y-axis intercepts: $R^2 = (0.0, 0.21)$, $Q^2 = (0.0, -0.30)$. *n* = 9/group. **(E)** OPLS-DA loadings plot showing the TAG influence on the separation between the HP and C groups. TAGs elevated in HP are displayed on the positive side of the predictive component, whilst TAGs elevated in C are displayed on the negative. Red circles represent scTAGs. **(F)** Box plots showing the range of saturated scTAGs in C- (blue) and HP-fed (red) individuals). Data are presented as mean ± SEM and analysed by two-way repeated measures ANOVA with post-hoc Sidak's multiple comparisons test; * = $p \leq 0.05$, *n* = 9/group.

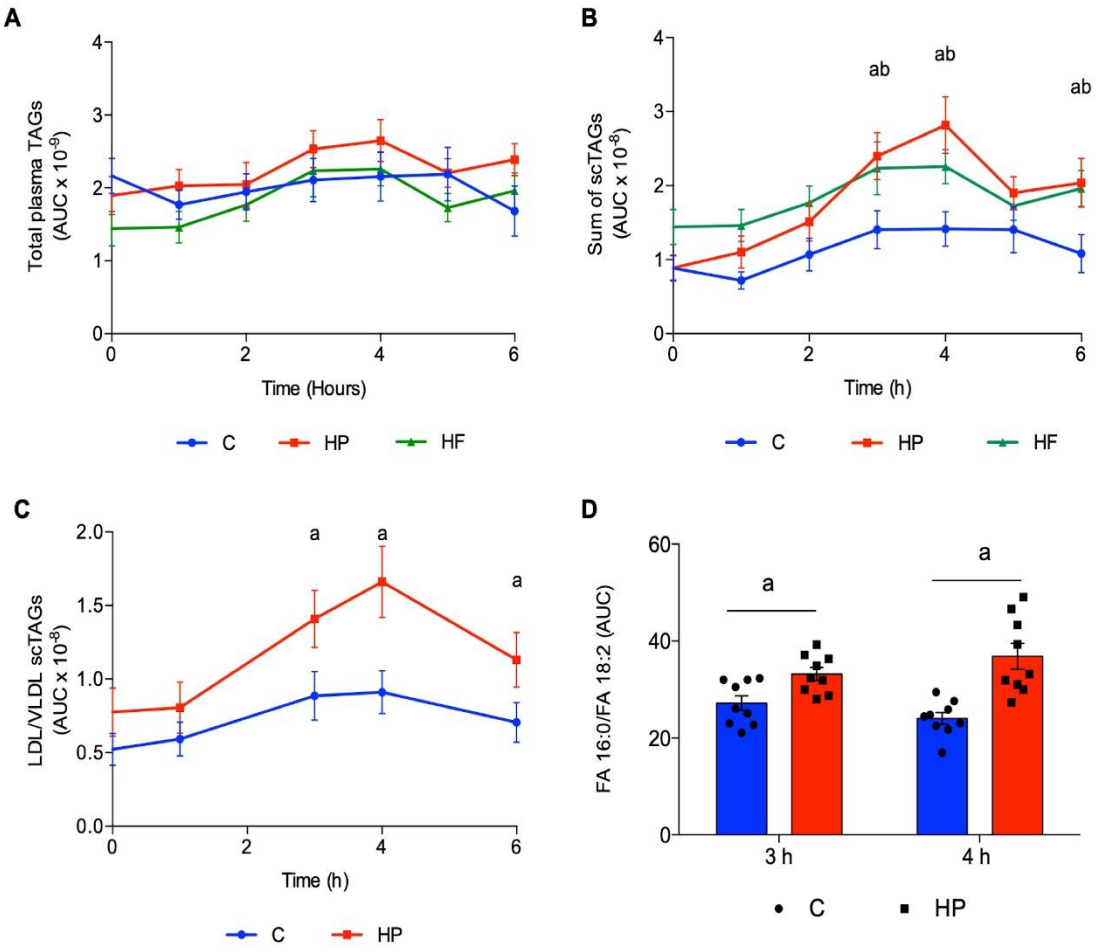

Figure 3. scTAGs are increased in plasma and plasma LDL/VLDL fraction after a HP meal in healthy human subjects. (A) Fasting (baseline; 0 h) and postprandial total TAG abundance in plasma after C (blue), HP (red) and HF (green) meal measured by LC-MS in samples drawn over 6 h. **(B)** Fasting (baseline; 0 h) and postprandial sum of scTAG abundance in plasma after C (blue), HP (red) and HF (green) meal measured by LC-MS in samples drawn over 6 h. **(C)** Fasting (baseline; 0 h) and postprandial LDL/VLDL scTAG abundance in plasma after C (blue)and HP (red) meal measured by LC-MS in samples drawn over 6 h. **(D)** DNL index reflected by the ratio of FA 16:0 to FA 18:2 after C (blue) and HP (red) meal at 3 h and 4 h. Data are presented as mean ± SEM and analysed by two-way repeated measures ANOVA with post-hoc Sidak's multiple comparisons test (**A**-**C**) or paired t-Test (**D**); a,b,c = $p \leq 0.05$, n = 9/group. a = comparisons between C and HP; b = comparisons between C and HF; C = comparisons between HP and HF.

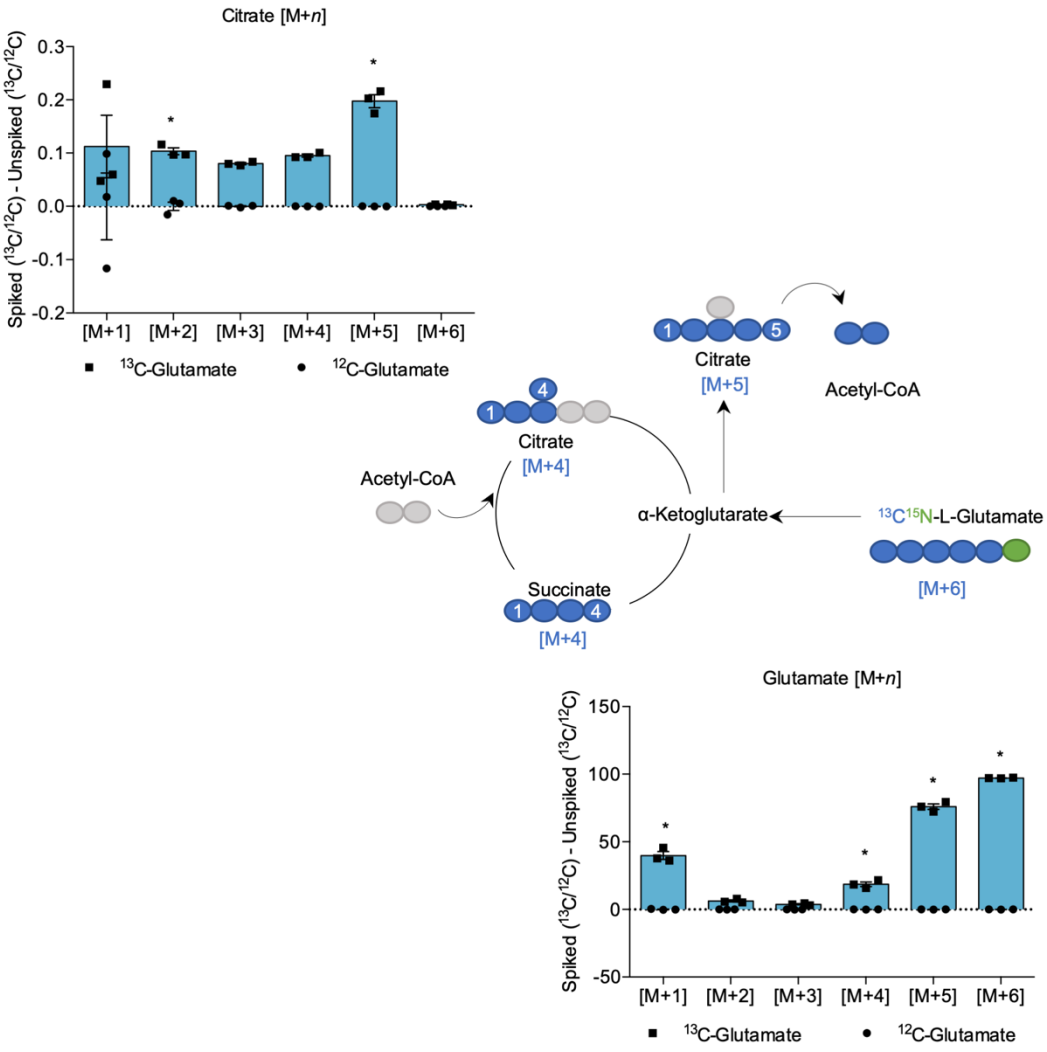

Figure 4. Carbon from $^{13}C_5$-labelled glutamate is incorporated into the TCA cycle in AML 12 hepatocytes. Labelling in glutamate and citrate, detected by LC-MS over 24 h post-supplementation. Data are presented as mean ± SEM and analysed by two-way ANOVA with post-hoc Sidak's multiple comparisons test ; * = $p \leq 0.05$, n = 3/group.

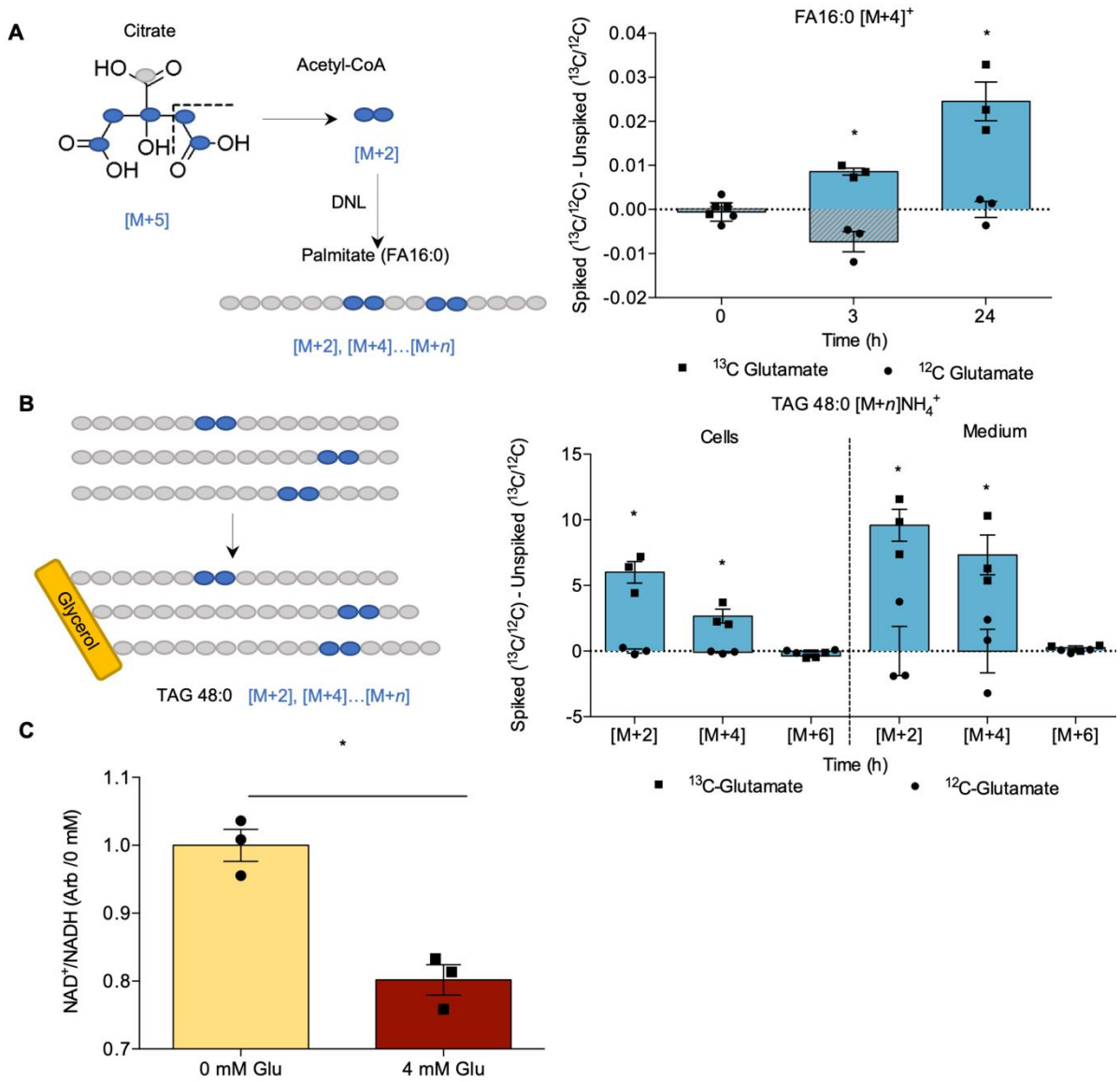

Figure 5. Carbon from $^{13}C_5$-labelled glutamate is incorporated into DNL-derived palmitate and triacylglycerols in AML 12 hepatocytes. (A) Labelling derived from glutamate in the $[M+4]^+$ ion of the picolynyl-ester of palmitate (FA16:0) generated by DNL, detected by LC-MS over 24 h post-supplementation. **(B)** Labelling derived from glutamate in the $[M+2]NH_4^+$, $[M+4]NH_4^+$ and $[M+6]NH_4^+$ ions of glyceryl tripalmitate (TAG 48:0) produced from DNL-derived palmitate in both cells and medium, detected by LC-MS after 24 h. **(C)** NAD^+/NADH at 0 mmol/L and 4 mmol/L glutamate after 24 h. Data are presented as mean ± SEM and analysed by two-way ANOVA with post-hoc Sidak's multiple comparisons test (**A**-**B**) or unpaired t-Test (**C**); * = $p \leq 0.05$, n = 3/group.

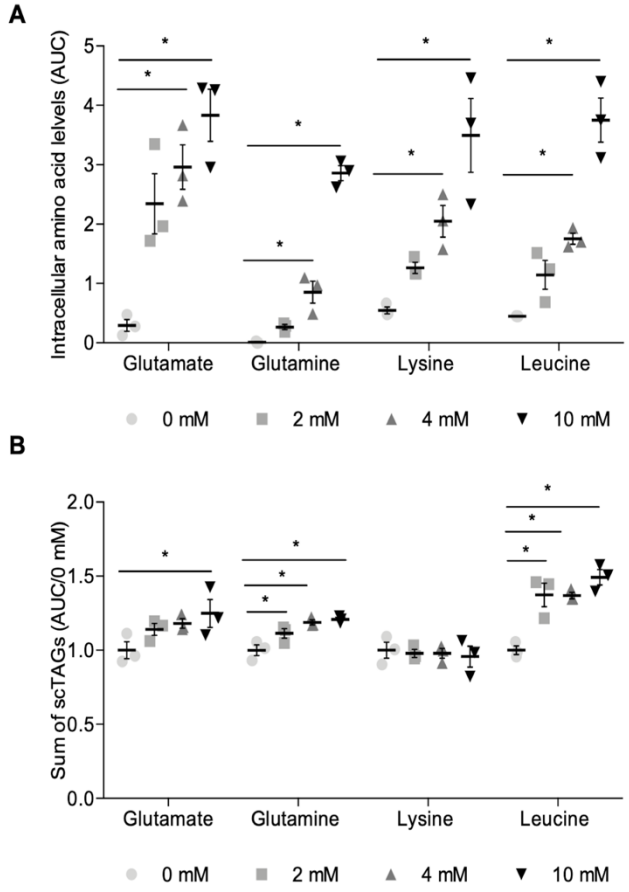

Figure 6. Intracellular scTAGs levels increase dose-dependently in response to glutamate, glutamine and leucine but not lysine concentrations in AML 12 hepatocytes. (A) Amino acid levels in cells in response to specific amino acid treatment at 0, 2, 4 and 10 mmol/L concentrations measured by LC-MS after 24 h. **(B)** Sum of scTAG content in cells in response to specific amino acid treatment at 0, 2, 4 and 10 mmol/L concentrations measured by LC-MS after 24 h. Data are presented as mean ± SEM and analysed by one-way ANOVA with post-hoc Dunnett's multiple comparisons test; * = $p \leq 0.05$, n = 3/group.

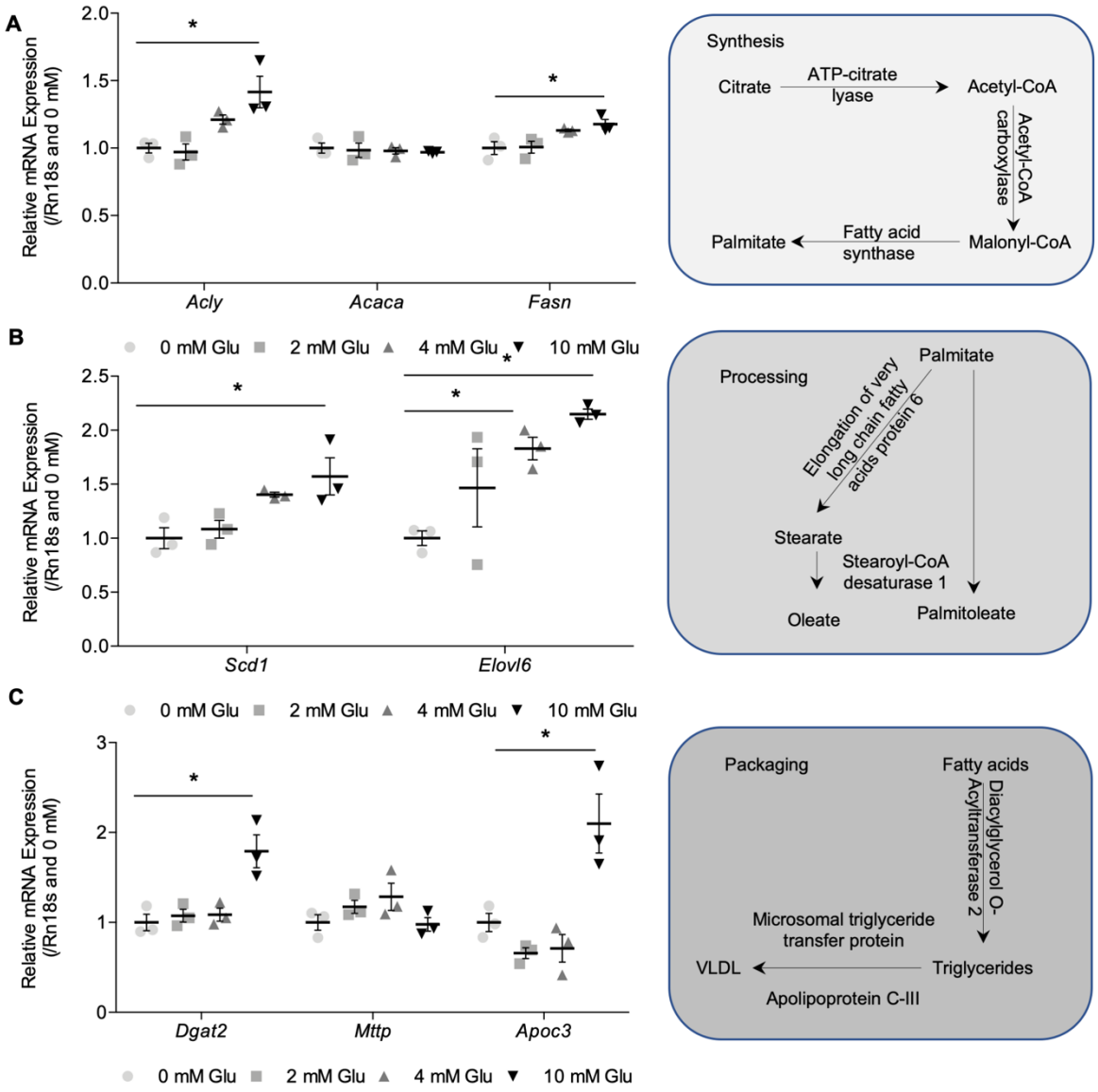

Figure 7. Increasing glutamate concentration increases DNL synthesis, processing and VLDL packaging gene expression for fatty acids in AML 12 hepatocytes. (A) qPCR analysis of expression of DNL synthesis genes *Acly*, *Acaca* and *Fasn* after 24 h. **(B)** qPCR analysis of expression of processing genes *Scd1* and *Elovl6* after 24 h. **(C)** qPCR analysis of expression of packaging genes *Dgat2*, *Mttp* and *Apoc3* after 24 h. Data are presented as mean ± SEM and analysed by one-way ANOVA with post-hoc Dunnett's multiple comparisons test; * = $p \leq 0.05$, n = 3/group.

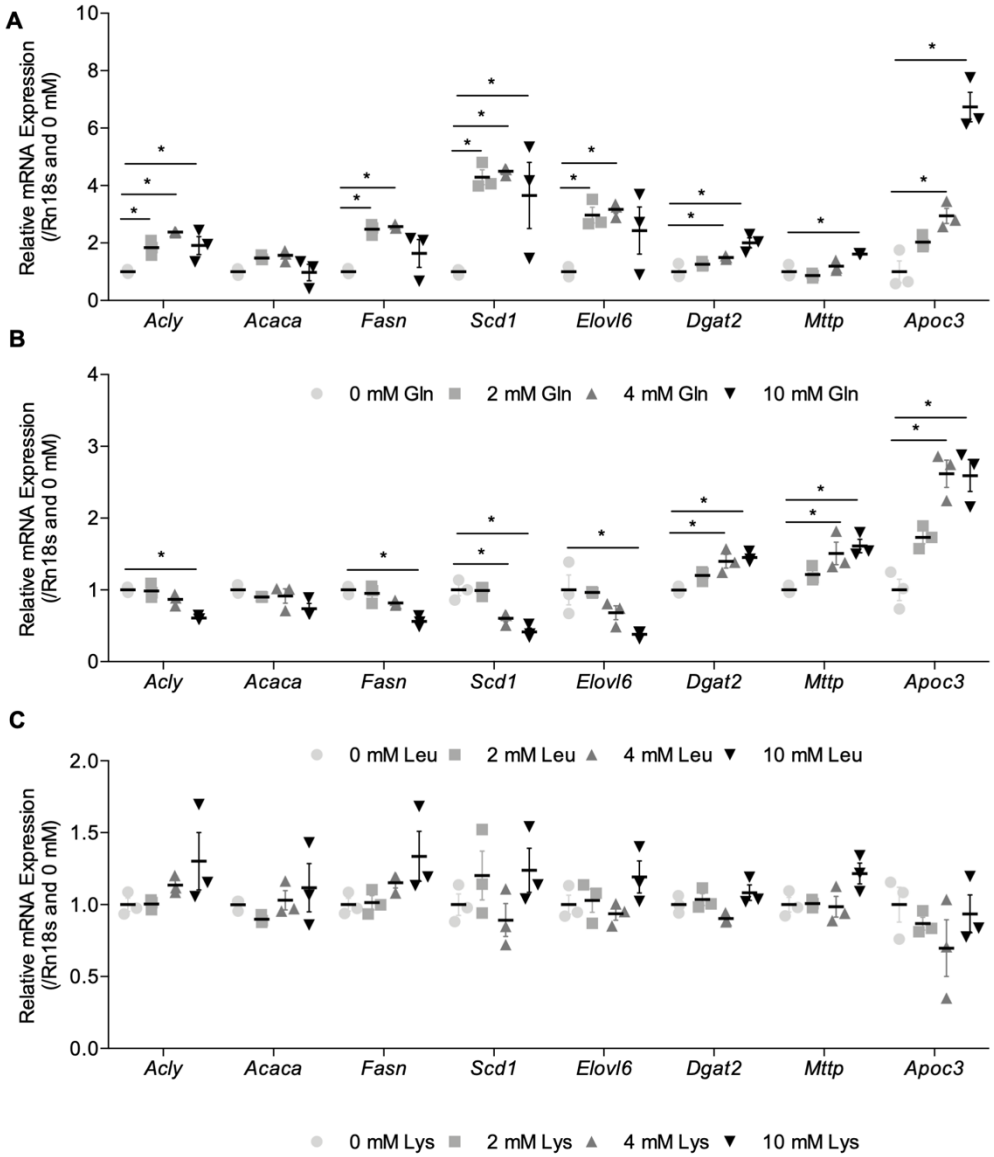

Figure 8. The effect of increasing glutamine, leucine and lysine concentrations on DNL synthesis, processing and VLDL packaging gene expression in AML 12 hepatocytes. (A) qPCR analysis of expression of *Acly*, *Acaca*, *Fasn*, *Scd1*, *Elovl6*, *Dgat2*, *Mttp* and *Apoc3* in response to 0, 2, 4 and 10 mmol/L glutamine after 24 h. **(B)** qPCR analysis of expression of *Acly*, *Acaca*, *Fasn*, *Scd1*, *Elovl6*, *Dgat2*, *Mttp* and *Apoc3* in response to 0, 2, 4 and 10 mmol/L leucine after 24 h. **(C)** qPCR analysis of expression of *Acly*, *Acaca*, *Fasn*, *Scd1*, *Elovl6*, *Dgat2*, *Mttp* and *Apoc3* in response to 0, 2, 4 and 10 mmol/L lysine after 24 h. Data are presented as mean ± SEM and analysed by one-way ANOVA with post-hoc Dunnett's multiple comparisons test; * = $p \leq 0.05$, n = 3/group.

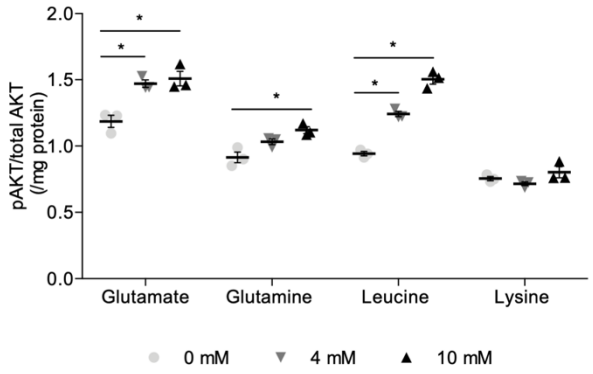

Figure 9. Intracellular pAKT levels increase dose-dependently in response to glutamate, glutamine and leucine but not lysine concentrations in AML 12 hepatocytes. Analysis of AKT activation as a function of AKT^{pS473} levels detected by ELISA after 24 h of amino acid supplementation. Data are presented as mean ± SEM and analysed by one-way ANOVA with post-hoc Dunnett's multiple comparisons test; * = $p \leq 0.05$, n = 3/group.

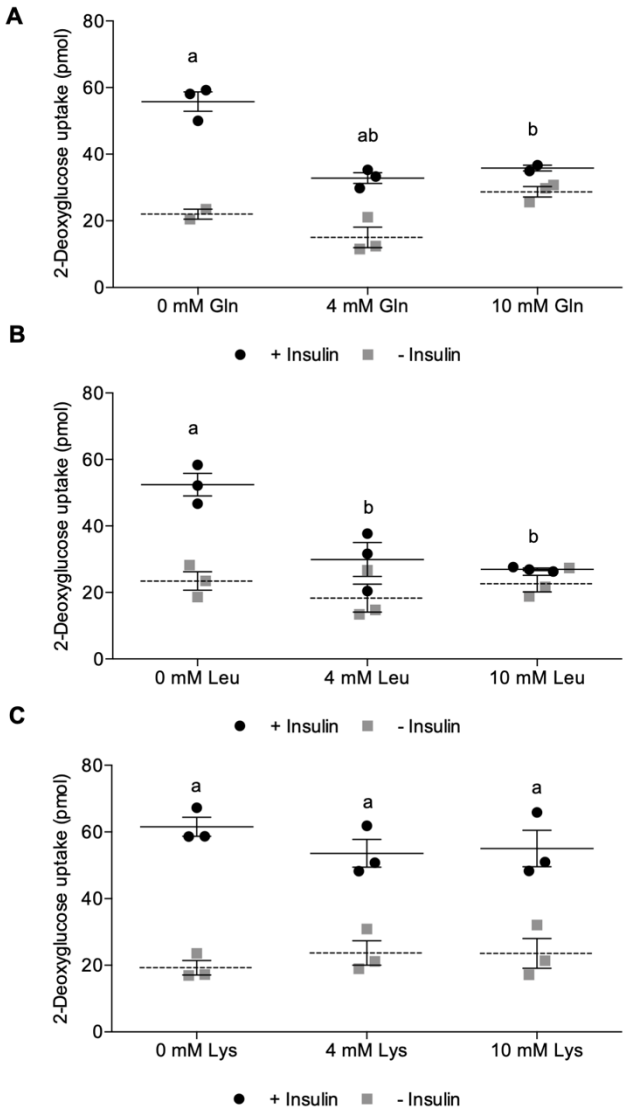

Figure 10. 2-deoxyglucose uptake decreases in response to glutamine and leucine but not lysine in AML 12 hepatocytes. (A) 2-deoxyglucose uptake assay on AML12 cells exposed to 0, 4 and 10 mmol/L glutamine for 24 h. **(B)** 2-deoxyglucose uptake assay on AML12 cells exposed to 0, 4 and 10 mmol/L leucine for 24 h. **(C)** 2-deoxyglucose uptake assay on AML12 cells exposed to 0, 4 and 10 mmol/L lysine for 24 h. Data are presented as mean ± SEM and analysed by two-way ANOVA with post-hoc Sidak's multiple comparisons test; a, b = $p \leq 0.05$, n = 3/group. a = comparisons between ± insulin within same amino acid concentration; b = comparisons between different amino acid concentrations within insulin treatment versus 0 mmol/L.

Table 1. Participant clinical and biochemical characteristics

Anthropometric Parameter	***Units***	***Mean***	***Standard Deviation***	***Range***
Age	Years	24.67	4.24	19-29
Weight	Kg	72.44	7.38	65.5-88.7
Height	m	179.03	7.74	167.8-191.5
BMI	kg/m^2	22.66	2.58	18.9-27.5
Systolic BP	mmHg	123.33	8.41	100-140
Diastolic BP	mmHg	71.11	8.54	50-85
Haematology				
White blood cell (WBC)count	$10^9/L$	5.03	0.54	3.9-10.2
Red blood cell (RBC) count	$10^{12}/L$	5.10	0.31	4.30-5.75
Haemoglobin (Hb)	g/L	146.89	4.70	135-172
Haematocrit (Hct)	L/L	0.45	0.02	0.395-0.505
Mean cell volume (MCV)	fL	87.40	5.63	80.0-99.0
Mean cell haemoglobin (MCH)	pg	28.83	2.08	27.0-33.5
Red cell distribution width (RDW)	%	13.06	0.79	11.0-16.0
Platelet (PLT) count	$10^9/L$	230.44	28.08	150-370
Platelet Haematocrit (PCT)	L/L	0.20	0.02	0.19-0.29
Mean Platelet volume (MPV)	fL	8.67	0.87	
Neutrophil count	$10^9/L$	2.74	0.58	1.50-7.70
Lymphocyte count	$10^9/L$	1.48	0.34	1.10-4.50
Monocyte count	$10^9/L$	0.35	0.11	0.10-0.90
Eosinophil count	$10^9/L$	0.09	0.04	0.02-0.50
Basophil count	$10^9/L$	0.03	0.02	0.00-0.20
Lipid profile, insulin and glucose				
Cholesterol	mmol/L	4.16	0.70	< 5
Triglyceride	mmol/L	0.88	0.36	0.3-1.80
HDL Cholesterol	mmol/L	1.39	0.16	> 1
LDL cholesterol	mmol/L	2.37	0.61	< 2.59
Cholesterol/HDL Ratio		3.02	0.74	< 3.5
Non HDL Cholesterol	mmol/L	2.77	0.74	<2.95
Insulin	pmol/l	36.33	16.66	0-80
Serum Glucose	mmol/L	4.47	0.33	3.9-5.5
Liver function				
Albumin	g/L	42.8	3.14	35-50
Total Bilirubin	umol/L	15.0	4.12	0-20
Alkaline Phosphatase	U/L	65.3	12.82	30-130
Alanine Transaminase	U/L	20.5	5.72	7-40
Gamma Glutamyltransferase	U/L	16.1	4.22	0-72

Table 2. Exclusion criteria of the human study

Exclusion criteria	Inclusion criteria
Smokers	Non-smoker males
BMI ≤18.5 and ≥ 27.5kg/m^2	BMI 18.5-27.5
Allergy or intolerance to any component of test meals	No allergy or intolerance to any component of the meals
Known history of cardiovascular disease	No history of cardiovascular disease
Impaired fasting glucose (fasting glucose ≥ 6.1 mmol/L)	Fasting glucose ≤ 6.1 mmol/L
Cholesterol ≥ 7.7 mmol/L	Cholesterol ≤ 7.7 mmol/L
Triglycerides ≥ 2.3 mmol/L	Triglycerides ≤ 2.3 mmol/L
Weight reduction medicines, anti-dyslipidemic agents	No weight reduction medicines or anti-dyslipidemic agents
Chronic, acute or active metabolic (including type 1 and type 2 diabetes mellitus) and inflammatory condition, haematological disorders, or any other systemic illness of renal, hepatic or gastrointestinal origin	No chronic, acute or active metabolic (including type 1 and type 2 diabetes mellitus) and inflammatory condition, haematological disorders, or any other systemic illness of renal, hepatic or gastrointestinal origin
Acute and chronic conditions affecting gastrointestinal motility	No acute and chronic conditions affecting gastrointestinal motility
Fat maldigestion and malabsorption	No fat maldigestion and malabsorption
The use of medication known to affect gastrointestinal motility (such as antiemetic, cathartics, antidiarrheal, anticholinergic and narcotic medication)	No use of medication known to affect gastrointestinal motility (such as antiemetic, cathartics, antidiarrheal, anticholinergic and narcotic medication)
History of mental illness	No history of mental illness
History of substance abuse or alcoholism	No history of substance abuse or alcoholism
Current self-reported weekly alcohol intake exceeding 14 units per week	Current self-reported weekly alcohol intake less than 14 units per week